NASA/CR-1999-209366

An Inviscid Computational Study of an X-33 Configuration at Hypersonic Speeds

Ramadas K. Prabhu
Lockheed Martin Engineering & Sciences Company, Hampton, Virginia

July 1999

The NASA STI Program Office ... in Profile

Since its founding, NASA has been dedicated to the advancement of aeronautics and space science. The NASA Scientific and Technical Information (STI) Program Office plays a key part in helping NASA maintain this important role.

The NASA STI Program Office is operated by Langley Research Center, the lead center for NASA's scientific and technical information. The NASA STI Program Office provides access to the NASA STI Database, the largest collection of aeronautical and space science STI in the world. The Program Office is also NASA's institutional mechanism for disseminating the results of its research and development activities. These results are published by NASA in the NASA STI Report Series, which includes the following report types:

- TECHNICAL PUBLICATION. Reports of completed research or a major significant phase of research that present the results of NASA programs and include extensive data or theoretical analysis. Includes compilations of significant scientific and technical data and information deemed to be of continuing reference value. NASA counterpart of peer-reviewed formal professional papers, but having less stringent limitations on manuscript length and extent of graphic presentations.
- TECHNICAL MEMORANDUM. Scientific and technical findings that are preliminary or of specialized interest, e.g., quick release reports, working papers, and bibliographies that contain minimal annotation. Does not contain extensive analysis.
- CONTRACTOR REPORT. Scientific and technical findings by NASA-sponsored contractors and grantees.
- CONFERENCE PUBLICATION. Collected papers from scientific and technical conferences, symposia, seminars, or other meetings sponsored or co-sponsored by NASA.
- SPECIAL PUBLICATION. Scientific, technical, or historical information from NASA programs, projects, and missions, often concerned with subjects having substantial public interest.
- TECHNICAL TRANSLATION. English-language translations of foreign scientific and technical material pertinent to NASA's mission.

Specialized services that complement the STI Program Office's diverse offerings include creating custom thesauri, building customized databases, organizing and publishing research results ... even providing videos.

For more information about the NASA STI Program Office, see the following:

- Access the NASA STI Program Home Page at ***http://www.sti.nasa.gov***
- E-mail your question via the Internet to help@sti.nasa.gov
- Fax your question to the NASA STI Help Desk at (301) 621-0134
- Phone the NASA STI Help Desk at (301) 621-0390
- Write to:
  NASA STI Help Desk
  NASA Center for AeroSpace Information
  7121 Standard Drive
  Hanover, MD 21076-1320

NASA/CR-1999-209366

An Inviscid Computational Study of an X-33 Configuration at Hypersonic Speeds

Ramadas K. Prabhu
Lockheed Martin Engineeering & Sciences Company, Hampton, Virginia

National Aeronautics and
Space Administration

Langley Research Center
Hampton, Virginia 23681-2199

Prepared for Langley Research Center
under Contract NAS1-96014

July 1999

Available from:

NASA Center for AeroSpace Information (CASI)
7121 Standard Drive
Hanover, MD 21076-1320
(301) 621-0390

National Technical Information Service (NTIS)
5285 Port Royal Road
Springfield, VA 22161-2171
(703) 605-6000

Summary

This report documents the results of a study conducted to compute the inviscid longitudinal aerodynamic characteristics of a simplified X-33 configuration. This study was conducted in support of the industry led X-33 program. The major components of the X-33 vehicle, namely the body, the canted fin, the vertical fin, and the bodyflap, were simulated in the CFD model. The rear-ward facing surfaces at the base including the aerospike engine surfaces were not simulated. The FELISA software package was used for this study. This software consists of an unstructured surface and volume grid generator and two inviscid flow solvers - one for transonic flows and the other for hypersonic flows. The hypersonic flow solver with perfect gas, equilibrium air, and CF_4 gas options was used in the present study. Computations were made for Mach 4.96, 6.0, and 10.0 with perfect gas air option, and for Mach 10 with equilibrium air option with flow condition of a typical point on the X-33 flight trajectory. Computations were also made with CF_4 gas option at Mach 6.0 to simulate the CF_4 tunnel flow condition. An angle of attack range of 12 to 48 deg. was covered. The CFD results were compared with available wind tunnel data. Comparison was good at low angles of attack; at higher angles of attack (beyond 25 deg.) some differences were found in the pitching moment. These differences progressively increased with increase in angle of attack, and are attributed to the viscous effects. However, the computed results showed the trends exhibited by the wind tunnel data.

Nomenclature

C_A	$\mathbf{F_A}/(q_\infty\ S_{ref})$, Axial force coefficient
C_N	$\mathbf{F_N}/(q_\infty\ S_{ref})$, Normal force coefficient
C_m	$\mathbf{M_y}/(q_\infty\ S_{ref}\ l_{ref})$, Pitching moment coefficient
C_p	$(p - p_\infty)/q_\infty$, Pressure coefficient
$\mathbf{F_A}$	Axial force
$\mathbf{F_N}$	Normal force
l_{ref}	Reference length, (=758.4 sq.in.)
$\mathbf{M_y}$	Pitching moment
M_∞	Freestream Mach number
p	Static pressure
p_∞	Freestream static pressure
q_∞	Freestream dynamic pressure
S_{ref}	Reference area, (=231,520.0 sq.in.)
x, y, z	Cartesian co-ordinates of a given point
α	Angle of attack, deg.

Geometry

The present computational study was done on the Lockheed X-33 F-loft, Rev. F configuration. The primary external components of this vehicle are the body, the canted fin, the vertical fin, the bodyflap, and the aerospike engines. All of these components, except the aerospike engine surfaces, were simulated in the CFD model. In order to preclude separated flow regions, mainly over the rearward facing areas like the base of

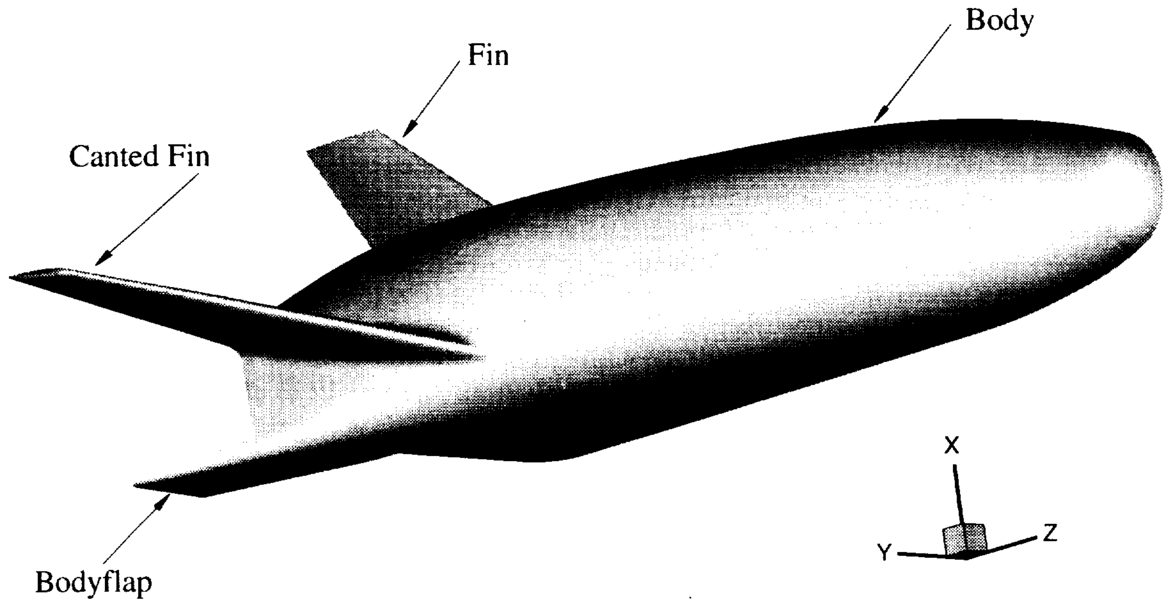

Figure 1: The X-33 F-loft Rev. F vehicle.

the vehicle, the flow over the base was not simulated. This was accomplished by extending the surfaces of the canted fin, vertical fin, and the of body downstream of the trailing edge so that they ended on a single surface. These extension surfaces provide a cover for the base. In the CFD computations, the flow was forced to be tangential to these extension surfaces. However, while computing the aerodynamic loads on the vehicle, these surfaces were ignored.

A sketch of the X-33 model used in the present CFD study is shown in Fig. 1. The axis system used for this study is also shown in the figure. The origin is at the nose of the vehicle with the z-axis along the body axis pointing upstream, y-axis perpendicular to the symmetry plane, and the x-axis in the symmetry plane perpendicular to the z-axis. The length of the body (from nose to trailing edge of the bodyflap) is approximately 831.1 in. and the tip-to-tip distance of the canted fins is 920.75 in. The canted fins make an angle of 72 deg. to the plane of symmetry. There are two vertical fins separated from each other by 200 in. For the present computations, the control surfaces, namely the rudder and the bodyflaps were in the undeflected position. Since the vehicle has a plane of symmetry, only one half of the vehicle was simulated in the computational model. The reference quantities used for reducing the aerodynamic loads to the non-dimensional form are as follows:

Reference area	231,520.0 sq.in.
Reference length	758.4 in.
Pitching moment reference point	(0.0, 0.0, -500.544) in.

Grid ID	No. of Tets	No. of Points	No. of Triangles	No. of Surface Points
X33A	7,955,084	1,337,224	242,850	121,427
X33C	6,506,154	1,094,694	203,160	101,582
X33D	7,069,961	1,189,736	220,066	110,035

Table 1: Properties of grids used in the present computations.

The Felisa Software

All the computations of the present study were done using the FELISA unstructured grid software. This software package consists of a set of computer codes for the simulation of three-dimensional steady inviscid flows using unstructured tetrahedral grids. Surface triangulation and discretization of the computational domain using tetrahedral elements is done by two separate codes. Two flow solvers are available--one applicable for transonic flows, and the other for hypersonic flows with an option for perfect gas air, equilibrium air, or CF_4 gases. The hypersonic flow solver was used for all the computations in this study. Post-processors like the aerodynamic analysis routine are part of the software package. More information on FELISA may be found in [1]. A description of the hypersonic flow solver may be found in [2].

Grids Used in the Present Study

Starting with a structured surface grid in the form of a PLOT3D file, and using the software GridTool [3], a set of FELISA data files was generated. This includes the body surface and the computational domain definition file, and a file that specifies the grid spacing. The grid spacings file was modified manually in order to obtain the desired grid spacing near the nose of the vehicle. Using these data files unstructured tetrahedral grids were generated with the FELISA volume grid generator. Three separate unstructured surface and volume grids were generated to suit the freestream conditions. The properties of these grids are shown in Table 1 above. All these grids were generated on an SGI ONYX located in the Aerothermodynamics Branch (AB), NASA Langley.

A minimum grid spacing was 0.4 inch was used near the nose of the body. A plot of a portion of the grid on the symmetry plane near the nose is shown in Fig. 2. The model surface triangulation for grid X33A is shown in Fig. 3.

Flow Conditions

The freestream conditions and the range of angles of attack covered in the present study are shown in Table 2. All perfect gas air computation (cases 1-12) were done with $\gamma = 1.4$. Freestream conditions for the equilibrium air computations (cases 13–15) corresponded to the conditions for a typical point on the X-33 flight trajectory. Some wind tunnel tests had been conducted on an X-33 model in the Langley 31-inch Mach 10 tunnel and also in the Langley Mach 6 CF_4 tunnel. In order to simulate the CF_4 tunnel tests, a set of computations was done (cases 18-21) with the CF_4 gas options and freestream conditions corresponding to the conditions in the CF_4 tunnel. The freestream conditions for computations at Mach 9.02 correspond to atmospheric flight at a nominal Mach number of 9 at an altitude of 133,000 ft., and the conditions for

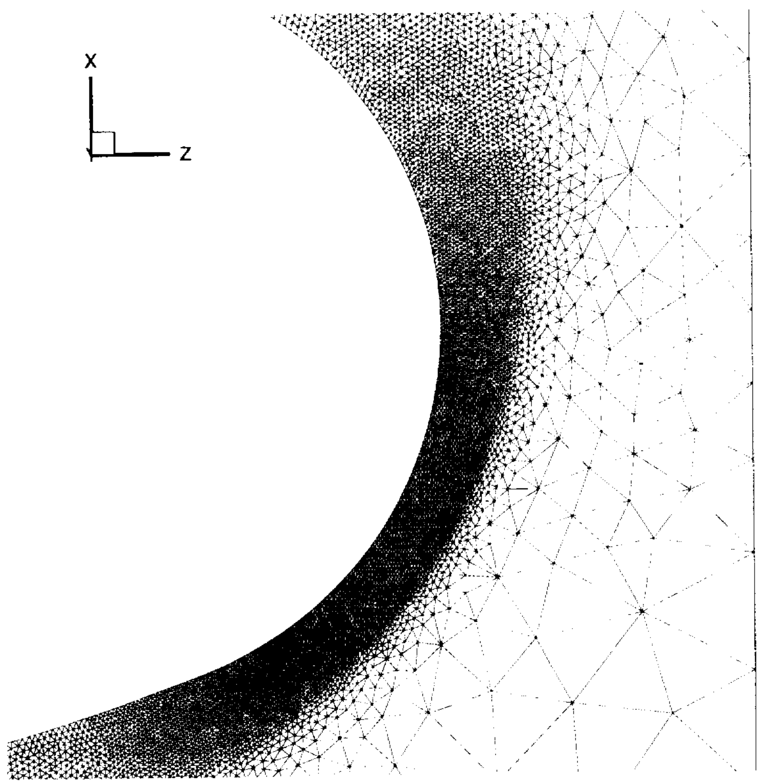

Figure 2: A typical triangulation on the symmetry plane near the nose of X-33.

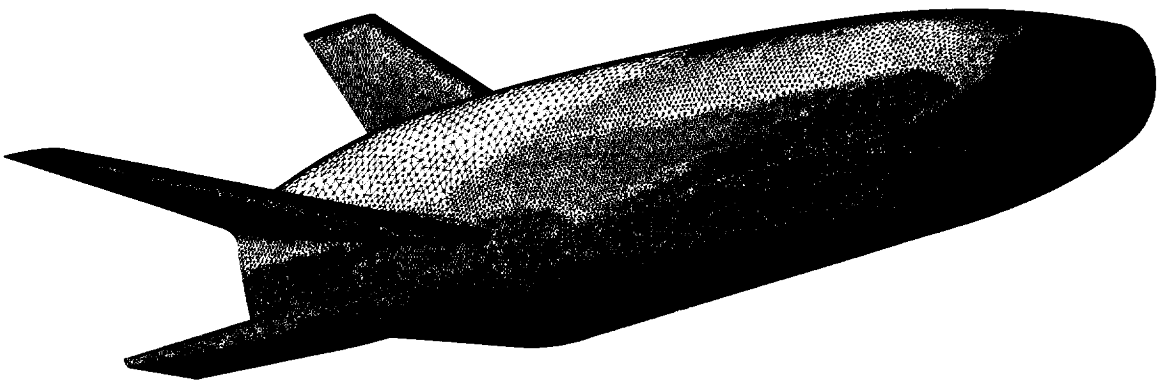

Figure 3: Surface triangulation for X33A grid.

Case No.	Mach No.	Gas Model	Density (Kg/m^3)	Temperature (Kelvin)	Velocity (m/sec)
1–4	10.0	Perfect Gas	NA	NA	NA
5 8	6.00	Perfect Gas	NA	NA	NA
9–12	4.96	Perfect Gas	NA	NA	NA
13–15	10.0	Equil. Air	4.3120E-04	259.5	3224
16	9.02	Equil. Air	3.6867E-03	251.9	2863
17	12.02	Equil. Air	1.0593E-03	270.7	3958
18–21	6.02	CF_4 gas	1.7700E-02	170.0	850

Table 2: Freestream conditions.

computations at Mach 12.02 correspond to atmospheric flight at a nominal Mach number of 12 at an altitude of 163,200 ft. These two cases correspond to two critical points in the flight trajectory of the X-33 vehicle.

Flow Solution

The flow solutions were computed on SGI Origin 2000 class parallel computers having 64 processors sitting on top of 16G of shared memory. The grids were partitioned so that the problem would run on eight processors. The FELISA hypersonic flow solver with the appropriate gas option was used for these flow computations. Each solution was started with the low-order option, and after a few hundred iterations, the higher-order option was turned on, and the solution was run to convergence. After every 20 iteration, the surface pressures were integrated, and the aerodynamic loads, namely the normal and the axial forces, and the pitching moment acting on the model were computed. The flow solution was assumed converged when these integrated loads reached steady values. Each solution required 32–40 hours of CPU time. The computed flow solutions were post-processed on the AB ONYX computer to obtain the aerodynamic loads. These loads were non-dimensionalized in the conventional manner, and the aerodynamic coefficients (C_N, C_A, and C_m) were obtained.

It should be recalled at this point that all the present computations are inviscid; hence the boundary layer and skin friction are absent. Absence of the skin friction leads to lower axial forces. Further, since the boundary layer is absent, the effects of boundary layer separation on the aerodynamic coefficients are not simulated. On the X-33, the flow would be fully separated over the base, and possibly over the upper surface of the bodyflap. These surfaces are not simulated in the present CFD model. These factors could introduce inaccuracies in the computed axial and normal forces, and as well as in the pitching moment.

Results and Discussion

The results of the present study are summarized in Table 3, and also shown graphically in Figures 4, 5, and 6. Tunnel test data in the form of curve fits for C_N, C_A, and C_m were available for the cases listed in the table 4. For the Mach 6 air case, the data at 4 million Reynolds number was chosen for comparison with the computed results.

The computed C_N and C_m for Mach numbers 4.96, 6, and 10 in perfect gas air are shown plotted Vs. α in Figure 4. Smooth curves have been drawn through the data points. The C_N Vs. α curves for the three cases shown in Fig. 4(a) have nearly the same slope. For a given α, the C_N values decrease as the Mach number is increased from 4.96 to 10.0. The pitching moment data for the three Mach numbers is shown in Fig. 4(b). For Mach 4.96 the C_m Vs. α has a large negative slope for α up to 35 deg.; beyond this angle of attack the slope becomes less negative. This indicates that the model is stable up to α=35 deg., beyond which it becomes less stable. For Mach 10, the trend is different. The slope of C_m Vs. α curve is nearly zero up to α=25 deg.; beyond this angle of attack the slope is negative. This indicates that the model is neutrally stable up to α=25 deg., beyond this angle of attack the vehicle becomes progressively more stable. The C_m Vs. α for Mach 6 lies in between the curves for Mach 4.96 and 10.0.

Computed C_N and C_m values for Mach 10 perfect gas air and equilibrium air are shown in Fig. 5. Tunnel data for Mach 10 are also plotted in this figure for comparison. Figure 5(a) shows that there is little difference between the computed C_N values for perfect gas air and the equilibrium air assumption. It should be recalled here that the freestream conditions for these equilibrium flow computations corresponded to those for a typical point on the X-33 flight trajectory. The total temperature under these conditions is 3040K. At this high temperature there would be considerable changes in the chemical composition and properties of air (see e.g. [4]). These changes do not seem to affect the normal force coefficient. The total temperature for the freestream conditions in the Mach 10 tunnel test section is only 980K. At this temperature there is very little change in the chemical composition of air; hence these tunnel data should be compared with perfect gas computations.

Figure 5(b) shows that there are some differences between computed C_m values for perfect gas and equilibrium air cases. These differences are due to the differences between the properties of perfect gas air and equilibrium air (at a total temperature of 3040K). However, there are significant differences between the computed and the wind tunnel C_m data. The differences are, although small at low angles of attack (0.001 up to α=30 deg.), increase as the angle of attack is increased (0.004 at α=48 deg.). This trend is possibly due to the viscous effects. On the wind tunnel model the flow on the upper surface of the canted fin would separate at high angles of attack due to the presence of the trailing edge shock. This would increase the pressures over the aft part of the canted fin, and, due to the large moment arm, result in positive pitching moment.

The computed C_N and C_m for Mach 6 perfect gas air and CF_4 gas are shown in Figs. 6(a) and (b) respectively, along with the test data from Langley 20-Inch Mach 6 Air tunnel and Langley Mach 6 CF_4 tunnel. The freestream conditions for the CF_4 gas computations corresponded to those in the Langley Mach 6 CF_4 tunnel test section with a total temperature of 980K. Figure 6(a) shows that the assumption of CF_4 gas at Mach 6 does not affect the computed normal force. Further, there is good agreement between the computations and the CF_4 tunnel data. However, there are differences between the computed results and the air tunnel data. In the past C_N values computed using FELISA had compared well with tunnel data; see for example [5]. The differences noticed in the present case could not be explained.

The computed C_m values for perfect gas air and CF_4 gas cases for Mach 6 are shown in Fig. 6(b). It may be observed that there are differences between the C_m values for the two cases. This is primarily due to the fact that air and CF_4 gas have different thermodynamic properties. For example, the density ratios across a normal shock at Mach 6 in CF_4 gas is about 10 compared to a value of about 5.3 in air. The pressure distribution over the vehicle for the CF_4 gas and in perfect gas air would be different. The tunnel test data is also shown in Fig. 6(b). It may be noticed from this figure that the computed C_m for CF_4 gas compares with the tunnel data up to about α=30 deg. Beyond this angle, the tunnel data exhibits less nose down C_m

Case No.	Mach No.	α, deg.	Gas Model	C_N	C_A	C_m
1	10.0	24	P.G. Air	0.4534	0.1033	0.0105
2	10.0	36	P.G. Air	0.8922	0.1014	0.0037
3	10.0	48	P.G. Air	1.3245	0.0919	-0.0033
4	10.0	12	P.G. Air	0.1232	0.1048	0.0111
5	6.00	24	P.G. Air	0.4898	0.1030	0.0089
6	6.00	36	P.G. Air	0.9252	0.0998	0.0032
7	6.00	48	P.G. Air	1.3401	0.0909	-0.0002
8	6.00	12	P.G. Air	0.1434	0.1065	0.0118
9	4.96	24	P.G. Air	0.5146	0.1025	0.0082
10	4.96	36	P.G. Air	0.9481	0.0979	0.0030
11	4.96	48	P.G. Air	1.3555	0.0881	0.0012
12	4.96	12	P.G. Air	0.1579	0.1071	0.0123
13	10.0	36	Equil. Air	0.8853	0.1079	0.0048
14	10.0	48	Equil. Air	1.3286	0.1040	-0.0041
15	10.0	24	Equil. Air	0.4484	0.1070	0.0113
16	9.02	20	Equil. Air	0.3279	0.1062	0.0116
17	12.02	35	Equil. Air	0.8318	0.1092	0.0060
18	6.02	12	CF_4 Gas	0.1458	0.1090	0.0118
19	6.02	24	CF_4 Gas	0.4763	0.1065	0.0116
20	6.02	36	CF_4 Gas	0.9044	0.1057	0.0059
21	6.02	48	CF_4 Gas	1.3526	0.0991	-0.0039

Table 3: Summary of computed aerodynamic coefficients for X-33.

Tunnel	Mach No.	Reynolds No.	α Range	Mount
Langley 20-Inch Mach 6 Air	6.0	0.5E+06	-4 to 48 deg.	Sting
Langley 20-Inch Mach 6 Air	6.0	2.0E+06	-4 to 48 deg.	Sting
Langley 20-Inch Mach 6 Air	6.0	4.0E+06	-4 to 48 deg.	Sting
Langley CF_4	6.0	0.4E+06	-4 to 48 deg.	Sting
Langley 31-Inch Air	10.0	2.0E+06	5 to 50 deg.	Blade

Table 4: Available wind tunnel data for X-33.

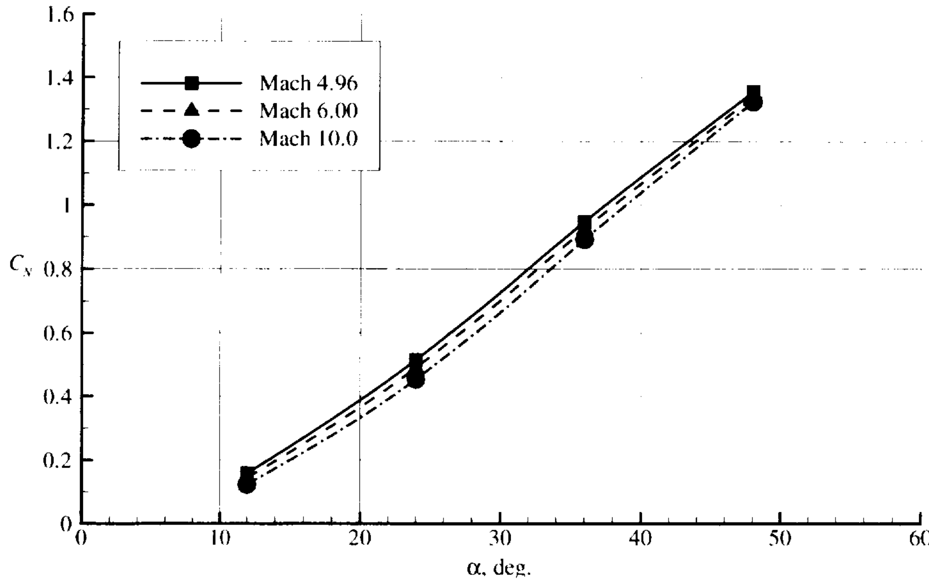

(a) C_N Vs. α

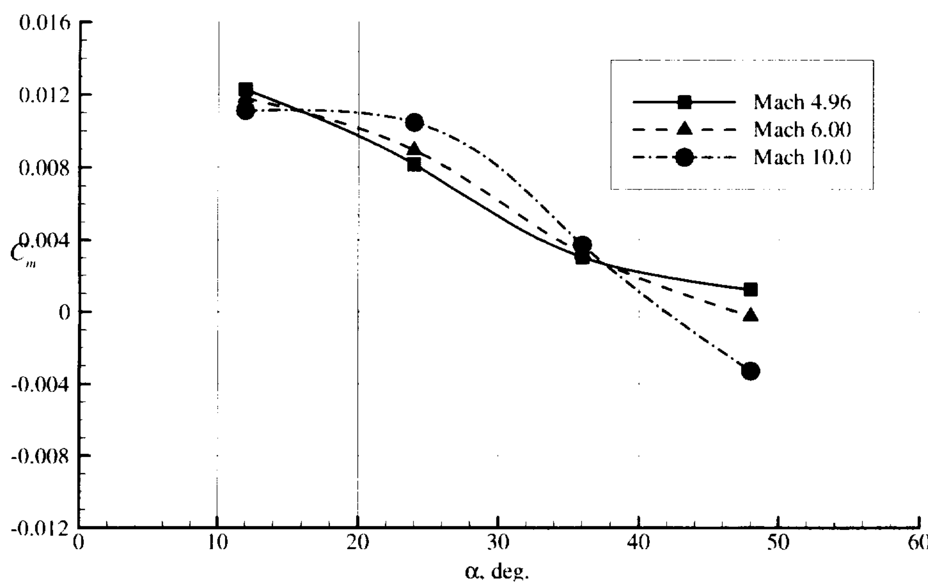

(b) C_m Vs. α

Figure 4: Computed C_N and C_m for X-33 in perfect gas air at Mach 4.96, 6.0, and 10.0.

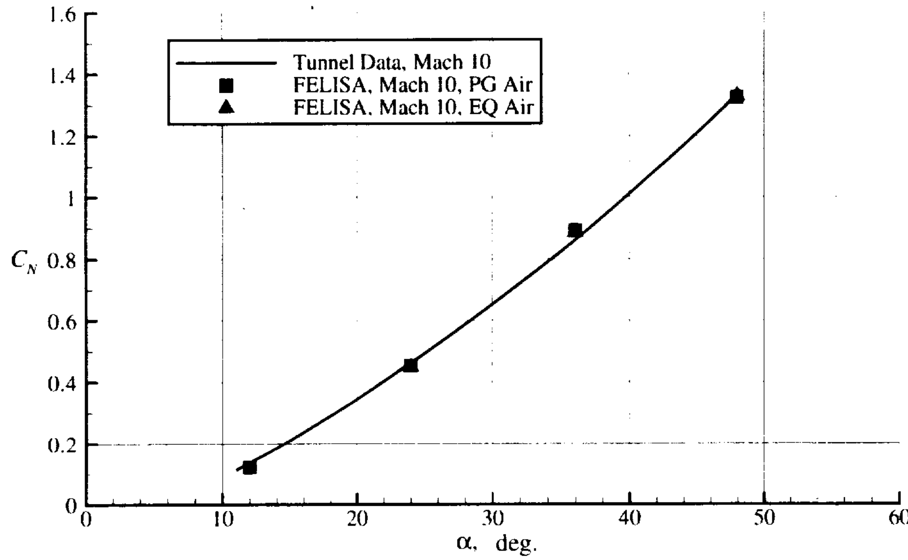

(a) C_N Vs. α

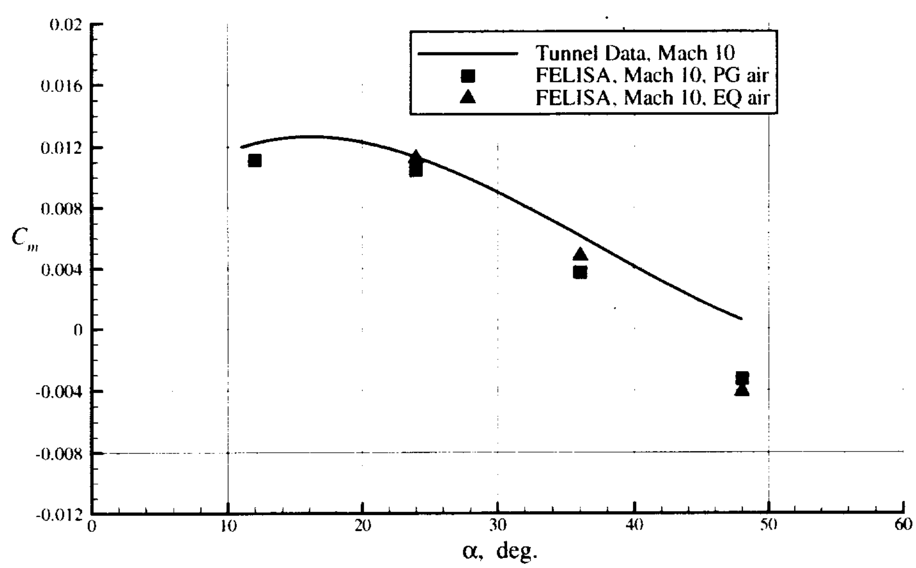

(b) C_m Vs. α

Figure 5: Comparison of computed and wind tunnel data for X-33 in perfect gas air and equilibrium air at Mach 10.0.

α	Body			Canted Fin			Bodyflap		
(deg.)	C_N	C_A	C_m	C_N	C_A	C_m	C_N	C_A	C_m
12	0.1221	0.0834	0.0137	0.1221	0.0834	0.0137	0.1221	0.0834	0.0137
24	0.3748	0.0931	0.0325	0.3748	0.0931	0.0325	0.3748	0.0931	0.0325
36	0.7182	0.1023	0.0518	0.7182	0.1023	0.0518	0.1067	-0.0025	-0.0242
48	1.0691	0.1050	0.0678	1.0691	0.1050	0.0678	0.1619	-0.0147	-0.0380

Table 5: Computed aerodynamic data for body, canted fin, and bodyflap, Mach 10, perfect gas air.

α	Body			Canted Fin			Bodyflap		
(deg.)	C_N	C_A	C_m	C_N	C_A	C_m	C_N	C_A	C_m
24	0.3715	0.0965	0.0329	0.0427	0.0094	-0.0095	0.0342	0.0010	-0.0122
36	0.7098	0.1085	0.0535	0.1058	-0.0018	-0.0240	0.0695	0.0012	-0.0247
48	1.0608	0.1170	0.0706	0.1655	-0.0138	-0.0386	0.1021	0.0008	-0.0361

Table 6: Computed aerodynamic data for body, canted fin, and bodyflap, Mach 10, equilibrium air

. For the perfect gas air case, the comparison is not as good. The difference increases progressively with increase in α for zero at α=12 deg. to 0.006 at α=48 deg.

In the Mach 6 and Mach 10 cases, the tunnel C_m values are invariably higher than the computed values at angles of attack 30 deg. and beyond. As noted earlier, this is possibly due to the effects of flow separation on the canted fin. The present computations are inviscid, as such there is no flow separation any surface, including the canted fins.

The contributions to C_N and C_m due to the body, canted fin, bodyflap, and the vertical fin were computed separately for all the cases. In all the cases the contributions from the vertical fin to C_N and C_m were found to be negligible. The contribution from the body, canted fin, and the bodyflap for Mach 10 perfect gas and Mach 10 equilibrium air cases are listed in Tables 5 and 6, and are also shown plotted in Figures 7 and 8. It may be noticed from these figures that body contributes the most to both normal force and pitching moment. The contributions of the canted fin and the bodyflap are of comparable magnitude.

Similarly, the results for Mach 6 perfect gas air and Mach 6 CF_4 gas cases are listed in Tables 7 and 8, and are also shown plotted in Figure 9 and 10.

Conclusion

Inviscid longitudinal aerodynamic characteristics of the Lockheed X-33 f-loft, Rev. F vehicle were computed for Mach 4.96, 6.0, and 10.0 over an angle of attack range of 4–48 deg. using the FELISA unstructured grid software package. The bodyflap and the rudder were in undeflected position. The canted fin, the vertical fin and the body surfaces were extended downstream in the computational model in order to preclude regions of separated flows. Computations were made for Mach 10 with the perfect gas air and equilibrium air

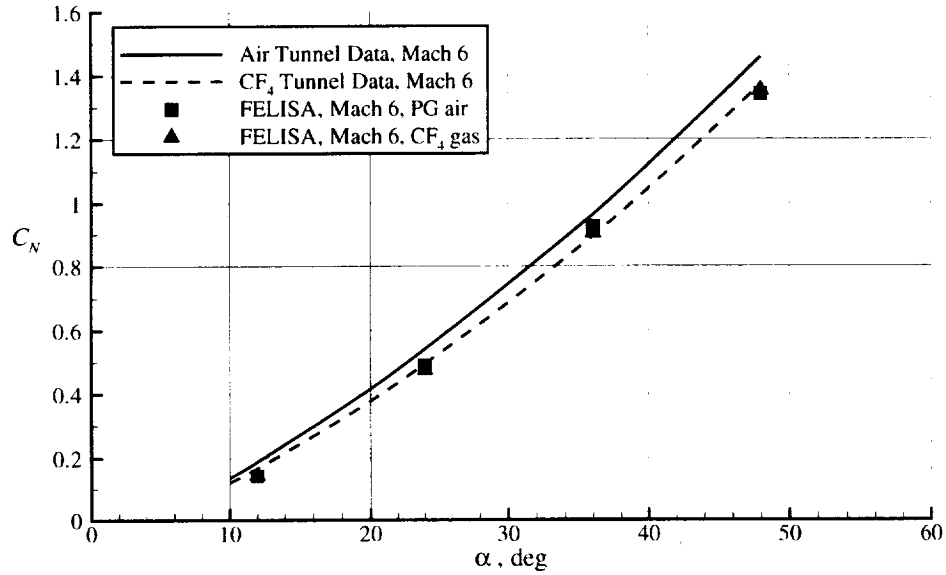

(a) C_N Vs. α

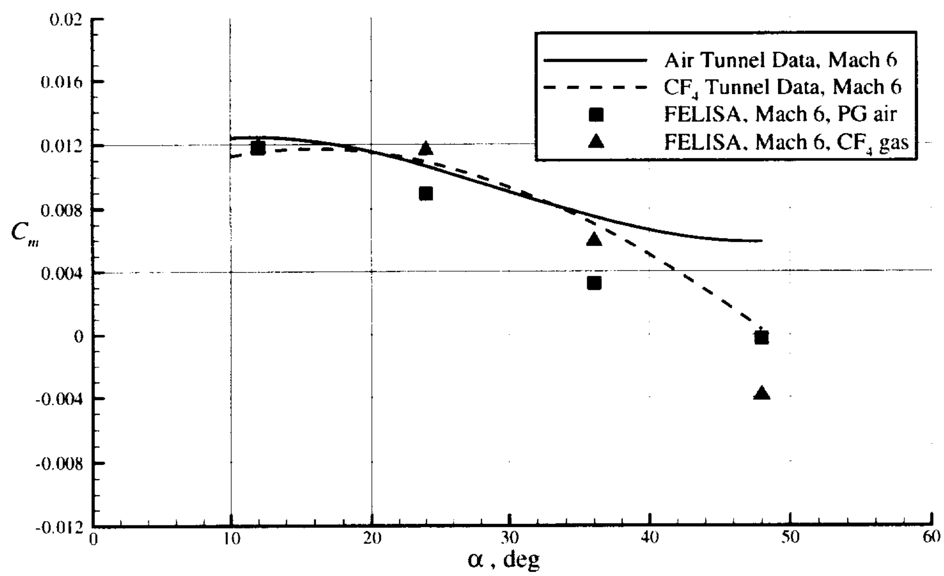

(b) C_m Vs. α

Figure 6: Comparison of computed C_N and C_m for X-33 in perfect gas air and CF_4 gas at Mach 6

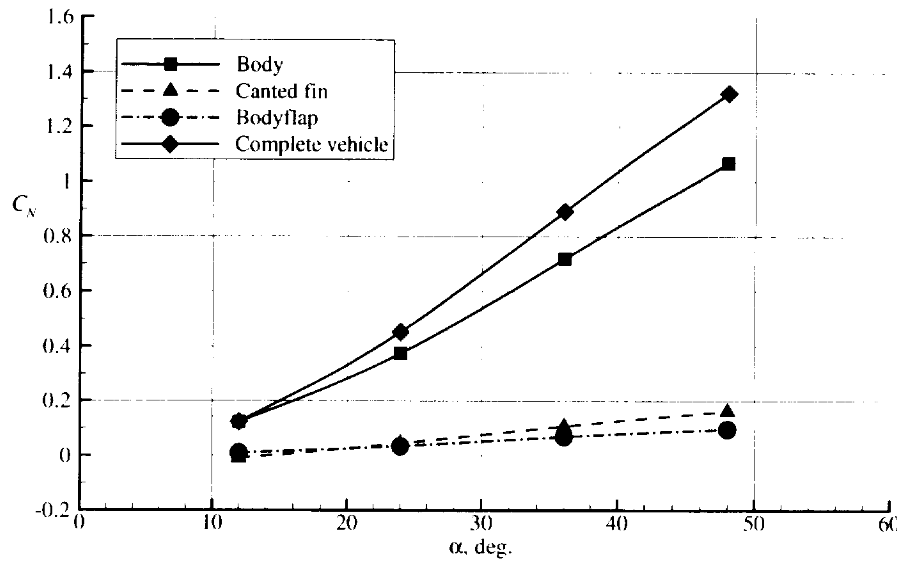

(a) C_N Vs. α

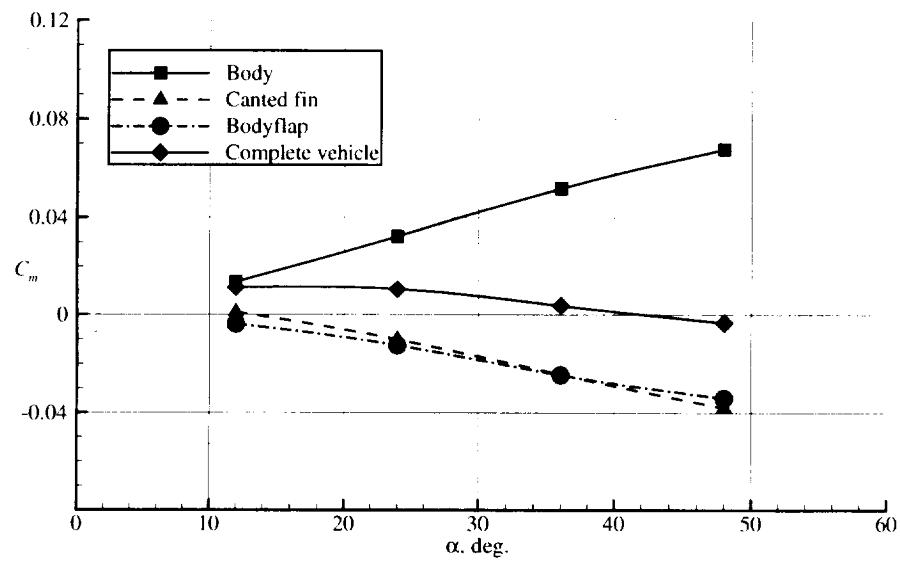

(b) C_m Vs. α

Figure 7: Computed C_N and C_m due to the body, canted fin, and bodyflap, and the complete vehicle for M=10, perfect gas air.

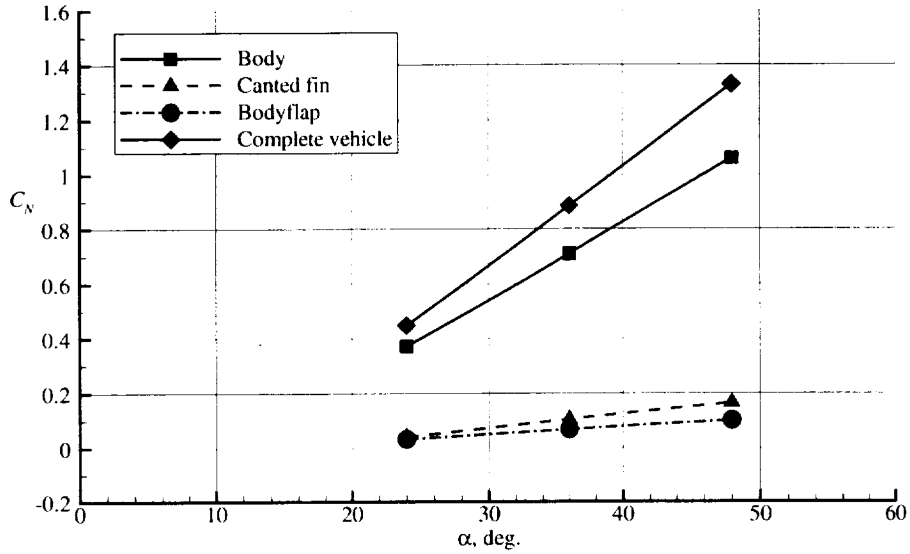

(a) C_N Vs. α

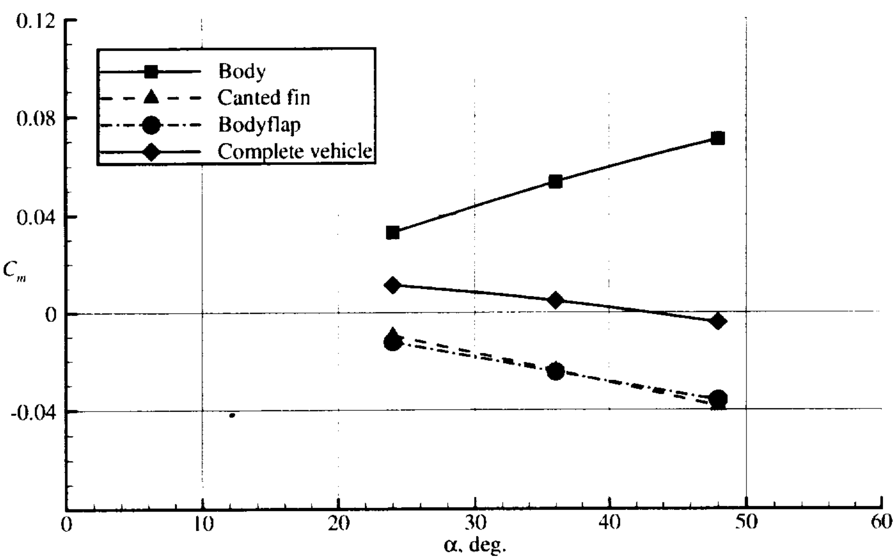

(b) C_m Vs. α

Figure 8: Computed C_N and C_m due to the body, canted fin, and bodyflap, and the complete vehicle for M=10, equilibrium air.

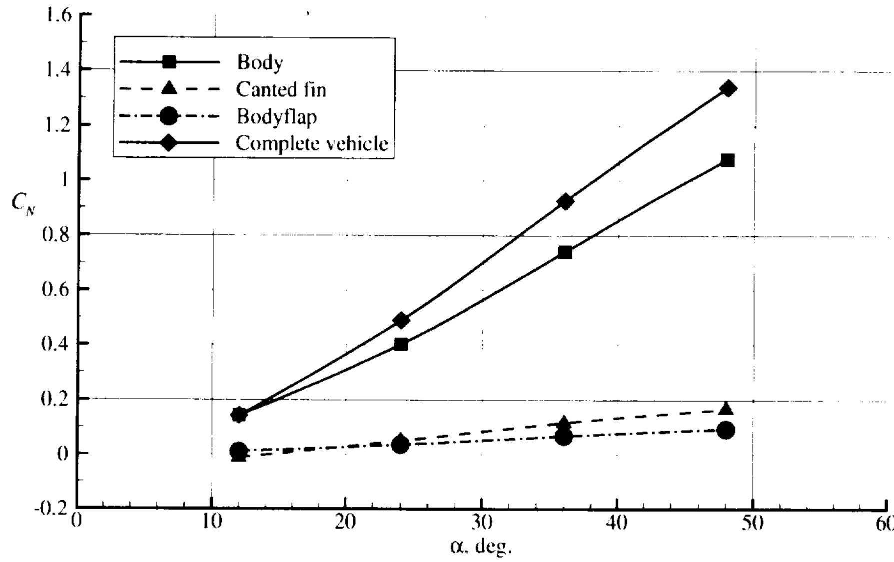

(a) C_N Vs. α

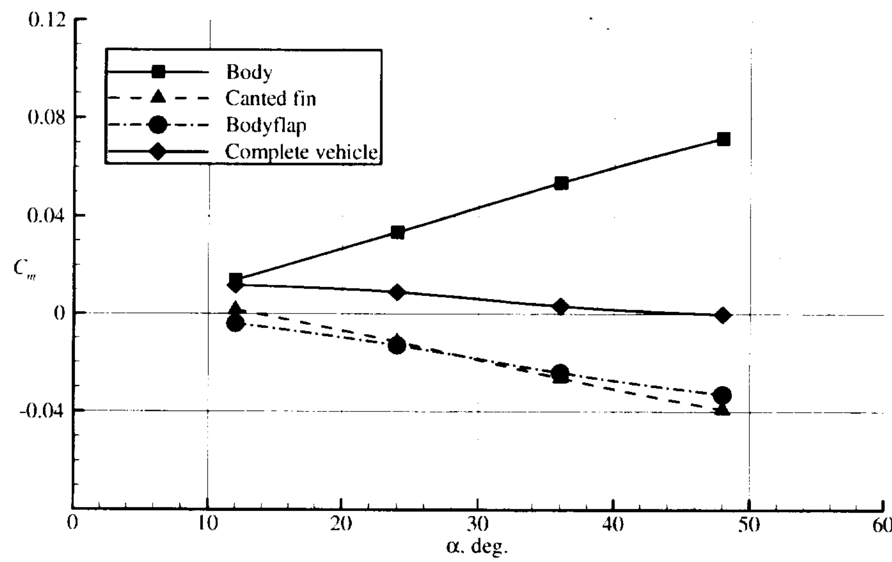

(b) C_m Vs. α

Figure 9: Computed C_N and C_m due to the body, canted fin, and bodyflap, and the complete vehicle for M=6, perfect gas air.

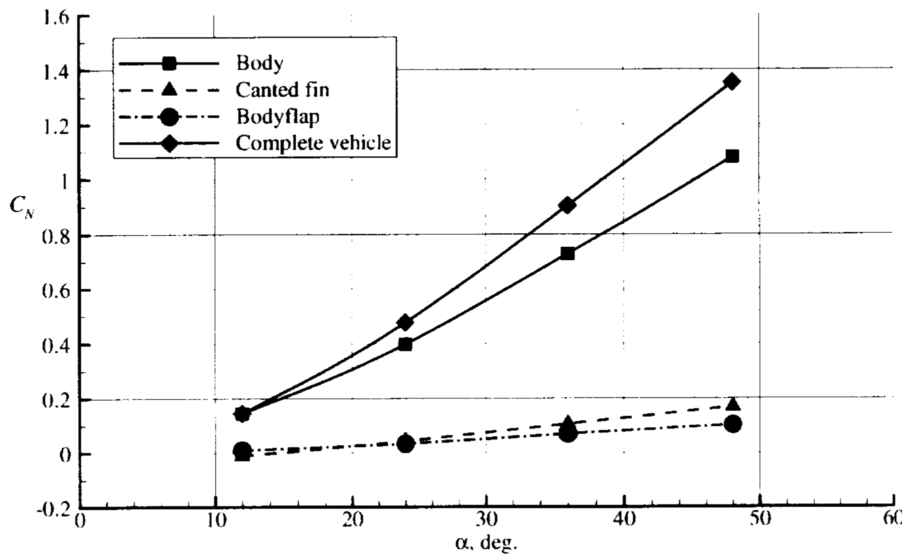

(a) C_N Vs. α

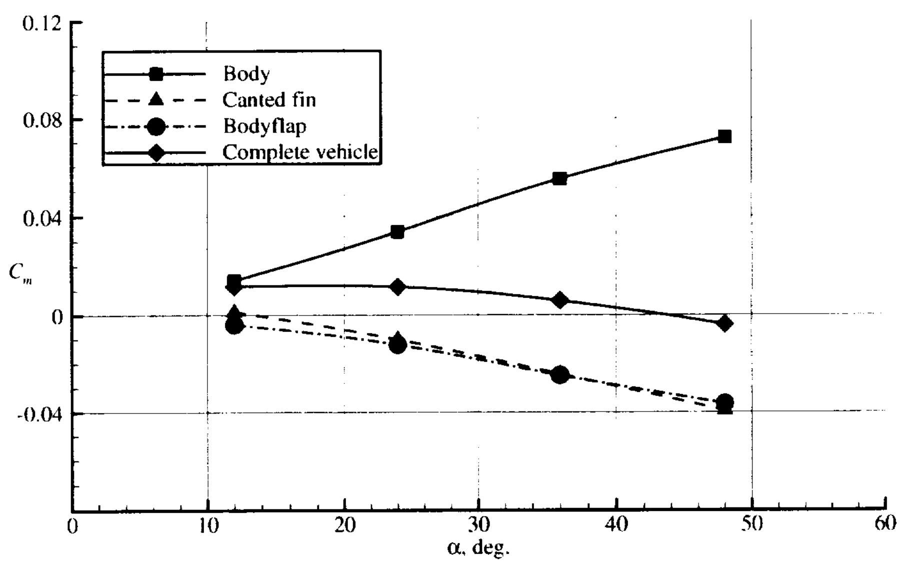

(b) C_m Vs. α

Figure 10: Computed C_N and C_m due to the body, canted fin, and bodyflap, and the complete vehicle for M=6, CF_4 gas.

α	Body			Canted Fin			Bodyflap		
(deg.)	C_N	C_A	C_m	C_N	C_A	C_m	C_N	C_A	C_m
12	0.1439	0.0848	0.0140	-0.0115	0.0202	0.0017	0.0113	0.0008	-0.0041
24	0.4018	0.0940	0.0336	0.0510	0.0078	-0.0116	0.0366	0.0010	-0.0130
36	0.7405	0.1029	0.0539	0.1159	-0.0042	-0.0264	0.0682	0.0011	-0.0242
48	1.0791	0.1065	0.0720	0.1670	-0.0162	-0.0391	0.0936	0.0001	-0.0330

Table 7: Computed aerodynamic data for body, canted fin, and bodyflap, Mach 6, perfect gas air.

α	Body			Canted Fin			Bodyflap		
(deg.)	C_N	C_A	C_m	C_N	C_A	C_m	C_N	C_A	C_m
12	0.1456	0.0873	0.0143	-0.0105	0.0202	0.0013	0.0110	0.0008	-0.0039
24	0.3977	0.0960	0.0339	0.0441	0.0093	-0.0100	0.0341	0.0010	-0.0122
36	0.7280	0.1058	0.0550	0.1062	-0.0015	-0.0242	0.0697	0.0013	-0.0247
48	1.0796	0.1118	0.0720	0.1695	-0.0138	-0.0393	0.1028	0.0008	-0.0309

Table 8: Computed aerodynamic data for body, canted fin, and bodyflap, Mach 6, CF_4 gas.

assumptions, and for Mach 6 with the perfect gas air and CF_4 gas assumptions. For the Mach 10 case, the computed C_N values compared well with the tunnel data. However, for the Mach 6 case, there were some differences. In the past C_N values computed using FELISA had compared well with tunnel data. See for example [5]. The differences noticed in the present case could not be explained.

The general trend of the C_m Vs. α curves noticed in the tunnel data are present the computed results. The computed pitching moment values for Mach 6 and 10 compared well with the tunnel data at low angles of attack. At higher angles of attack the tunnel data show gradual pitch-up compared to the computed results at both the Mach numbers. This is likely to be the result of flow separation on the upper surface of the canted fin. Flow separation occurs because of the the boundary layer interaction with the trailing edge shock. The present computations are inviscid; hence there is no flow separation. However, the trends of the tunnel data are predicted by the computations.

Acknowledgments

The work described herein was performed at Lockheed Martin Engineering & Sciences in Hampton, Virginia, and was supported by Aerothermodynamics Branch, NASA Langley Research Center under the contract NAS1-96014. The technical monitor was K. James Weilmuenster. The tunnel data in the form of curve fits was provided by Ms. Kelly Murphy of the Aerothermodynamics Branch.

References

[1] Peiro, J., Peraire, J., and Morgan, K., "FELISA System Reference Manual and User's Guide," Technical Report, University College, Swansea, Wales, 1993. NASA CP 3291, May 1995.

[2] Bibb, K.L., Peraire, J., and Riley, C.J.: "Hypersonic Flow Computation on Unstructured Meshes," AIAA Paper 97-0625, January 1997.

[3] Samereh, J., "GridTool: A Surface Modeling and Grid Generation Tool," NASA CP 3291, May 1995.

[4] Prabhu, R.K. and Erickson, W.F.: "A Rapid Method for the Computation of Equilibrium Chemical Composition of Air to 15000 K," NASA TP 2792, March 1988.

[5] Prabhu, R.K.: "Computational Study of a McDonnell Douglas Single-Stage-to-Orbit Vehicle Concept for Aerodynamic analysis," NASA CR 201606, September 1996.

REPORT DOCUMENTATION PAGE

Form Approved
OMB No. 0704-0188

1. AGENCY USE ONLY *(Leave blank)*	2. REPORT DATE	3. REPORT TYPE AND DATES COVERED
	July 1999	Contractor Report

4. TITLE AND SUBTITLE
An Inviscid Computational Study of an X-33 Configuration at Hypersonic Speeds

5. FUNDING NUMBERS
C NAS1-96014
WU 242-80-01-01

6. AUTHOR(S)
Ramadas K. Prabhu

7. PERFORMING ORGANIZATION NAME(S) AND ADDRESS(ES)
Lockheed Martin Engineering & Sciences Company
C/O NASA Langley Research Center
Hampton, VA 23681–2199

8. PERFORMING ORGANIZATION REPORT NUMBER

9. SPONSORING/MONITORING AGENCY NAME(S) AND ADDRESS(ES)
NASA Langley Research Center
Hampton, VA 23681–2199

10. SPONSORING/MONITORING AGENCY REPORT NUMBER
NASA/CR–1999–209366

11. SUPPLEMENTARY NOTES
Langley Technical Monitor: K. James Weilmuenster

12a. DISTRIBUTION/AVAILABILITY STATEMENT
Unclassified-Unlimited
Subject Category 02
Distribution: Nonstandard
Availability: NASA CASI (301) 621–0390

12b. DISTRIBUTION CODE

13. ABSTRACT *(Maximum 200 words)*
This report documents the results of a study conducted to compute the inviscid longitudinal aerodynamic characteristics of a simplified X-33 configuration. The major components of the X-33 vehicle, namely the body, the canted fin, the vertical fin, and the bodyflap, were simulated in the CFD model. The rear-ward facing surfaces at the base including the aerospike engine surfaces were not simulated. The FELISA software package consisting of an unstructured surface and volume grid generator and two inviscid flow solvers was used for this study. Computations were made for Mach 4.96, 6.0, and 10.0 with perfect gas air option, and for Mach 10 with equilibrium air option with flow condition of a typical point on the X-33 flight trajectory. Computations were also made with CF_4 gas option at Mach 6.0 to simulate the CF_4 tunnel flow condition. An angle of attack range of 12 to 48 deg. was covered. The CFD results were compared with available wind tunnel data. Comparison was good at low angles of attack; at higher angles of attack (beyond 25 deg.) some differences were found in the pitching moment. These differences progressively increased with increase in angle of attack, and are attributed to the viscous effects. However, the computed results showed the trends exhibited by the wind tunnel data.

14. SUBJECT TERMS	15. NUMBER OF PAGES
Unstructured grid, Hypersonic Speed, CFD, Aerodynamic Loads	23
	16. PRICE CODE
	A03

17. SECURITY CLASSIFICATION OF REPORT	18. SECURITY CLASSIFICATION OF THIS PAGE	19. SECURITY CLASSIFICATION OF ABSTRACT	20. LIMITATION OF ABSTRACT
Unclassified	Unclassified	Unclassified	UL